Magnetic phase diagram of the two-dimensional antiferromagnet $Ni_5(TeO_3)_4Br_2$

Matej Pregelj and Andrej Zorko
Institute Jožef Stefan, Jamova 39, 1000 Ljubljana, Slovenia

Oksana Zaharko
Laboratory for Neutron Scattering, ETHZ and Paul Scherrer Institute, CH-5232 Villigen, Switzerland

Rodolphe Bousier
LCMI, CNRS, 25 rue des Martyrs, 38042 Grenoble, France

Helmuth Berger
Institute of Physics of Complex Matter, EPFL, 1015 Lausanne, Switzerland

Hiroko A. Katori
Magnetic Materials Laboratory, Wako Institute, RIKEN, 351–0198 Saitama, Japan

Denis Arčon
Institute Jožef Stefan, Jamova 39, 1000 Ljubljana, Slovenia and Faculty of Mathematics and Physics, University of Ljubljana, Jadranska 19, 1000 Ljubljana, Slovenia

(Received 23 June 2008; revised manuscript received 9 December 2008; published 9 February 2009)

Phase diagram of the two-dimensional antiferromagnet $Ni_5(TeO_3)_4Br_2$ with triangular arrangement of Ni^{2+} ($S=1$) magnetic moments within the $[Ni_5O_{17}Br_2]$ subunits has been investigated by temperature and magnetic field dependent heat-capacity, magnetization, and magnetic-torque measurements down to 1.5 K and up to 23 T. A nonzero magnetic contribution to the heat capacity observed up to $2.3T_N$ is consistent with short-range magnetic ordering and the two-dimensional nature of the system. Below the Néel temperature $T_N=29$ K several antiferromagnetic phases were identified. The zero-field phase is characterized by a planar antiferromagnetic arrangement of the two in-layer neighboring $[Ni_5O_{17}Br_2]$ magnetic clusters within the magnetic unit cell. When the magnetic field is applied along the a^* crystal axis, a spin-flop-like transition to a phase with a complex out-of-plane arrangement of Ni^{2+} ($S=1$) magnetic moments occurs at ~ 10 T. Using a molecular-field approach we predict that this transition will shift to higher fields with increasing temperature and that a magnetic phase with ferromagnetic ordering of $[Ni_5O_{17}Br_2]$ magnetic clusters will occur above 24 T. We ascribe the richness of the magnetic phases to strongly exchange-coupled clusters, being the basic building blocks of the investigated layered system.

DOI: 10.1103/PhysRevB.79.064407 PACS number(s): 75.50.Ee, 81.30.Bx

I. INTRODUCTION

Two-dimensional (2D) antiferromagnetic (AFM) systems represent a fertile playground for experimental and theoretical investigations of phase transitions and critical phenomena. In recent years, they were intensively studied in relation to high-temperature superconductivity in cuprates,[1] colossal magnetoresistance in manganites,[2] and various exotic phases in geometrically frustrated lattices, with a kagome lattice as an archetype.[3] Phase diagrams of these systems are very rich and sensitively depend on a particular spin arrangement, magnetic anisotropy, and external perturbations, such as applied magnetic field or pressure.

Lately, 2D AFM systems that are built of strongly exchange-coupled magnetic clusters instead of individual magnetic moments have become accessible. Their phase diagrams, influenced by the competition between intracluster and intercluster interactions, are expected to be even more complex. The recently discovered compound,[4] $Ni_5(TeO_3)_4Br_2$, can be regarded as a novel representative of such systems. Here, five magnetic Ni^{2+} ($S=1$) moments constitute the $[Ni_5O_{17}Br_2]$ basic building block in which they are arranged into two Ni^{2+} triangles connected with a common central Ni site.[5] $[Ni_5O_{17}Br_2]$ entities are linked via eight corners to four nearest neighbors, which then form a layered structure. The triangle-based structure of the $[Ni_5O_{17}Br_2]$ unit suggests a geometrical frustration if AFM interactions between nearest-neighbor Ni^{2+} moments are assumed. These moments are situated in three different severely distorted octahedral surroundings, implying strong magnetic anisotropy.[6] The dominant magnetic interactions between the Ni^{2+} are indeed antiferromagnetic, as indicated by high-temperature susceptibility data, implying a negative Curie temperature $\theta \approx -50$ K. The system exhibits a long-range Néel ordered state below $T_N=29$ K.[4–8] Consequently, the empirical frustration parameter, $|\theta|/T_N=1.7$, is rather small. Neutron magnetic diffraction and unusual temperature dependence of the antiferromagnetic resonance (AFMR) frequency,[6,9] however, suggest a very complicated temperature dependence of the Ni^{2+} sublattice magnetizations in the ordered phase. This reflects the importance of competition between various magnetic terms, possibly leading to intriguing magnetic structures as a function of temperature and external magnetic field.

TABLE I. Summary of parameters for $Ni_5(TeO_3)_4Br_2$ used in the calculation of magnetic free energy [Eq. (1)]. All units are in kelvin.

	J_1+J_5	J_2	J_3+J_4	J_6	D_1	D_2	D_3	$d_{1,2}$	$d_{2,3}$
x	−0.8	34.7	56.4	10.7	−0.8	−0.6	6.1	0	0
y	−19.6	18.4	49.6	2.0	−10.8	−2.4	4.0	−5.2	0.1
z	−1.2	5.8	12.6	25.4	11.6	3.0	−10.0	0	0

In order to be able to understand the low-temperature behavior and field dependence of the magnetic ordering in the $Ni_5(TeO_3)_4Br_2$ system, we performed a systematic study, including heat-capacity, magnetization, and magnetic-torque measurements. This allowed us to determine a magnetic phase diagram of this compound in the temperature range between 300 and 1.7 K and in magnetic fields from 0 up to 23 T. Below T_N, several different AFM phases were identified and successfully explained with a molecular-field approach, developed in our previous AFMR report.[6] We stress that the observed richness of the phase diagram is a direct consequence of the competition between intracluster and intercluster exchange couplings on the one hand and single-ion magnetic anisotropy on the other hand.

II. EXPERIMENTAL DETAILS

Samples were synthesized by chemical vapor transport reaction, according to the procedure described in Ref. 6. After a four-week treatment in a two-zone gradient furnace, between 750 and 550 °C, orange-colored single-crystal plates with typical size of $10\times8\times0.2$ mm^3 were grown.

Heat-capacity measurements were performed on Quantum Design physical properties measurement system (PPMS) between 1.5 and 120 K in the applied magnetic fields of 0, 4, 6, and 9 T.

The magnetization response to the external magnetic field was recorded using two different techniques. First, the magnetization parallel to the applied magnetic field was measured with the Oxford instruments MagLab vibrating-sample magnetometer (VSM) from 0 to 12 T in the temperature range between 1.5 and 10 K. In order to detect magnetization perpendicular to the applied field, the magnetic-torque measurements were performed as a function of an applied field up to 23 T at several selected temperatures in the range between 1.7 and 40 K at the Grenoble High Magnetic Field Laboratory. A relative magnetic torque was determined from the capacity between a metallic cantilever holding the sample and a fixed metallic plate.[10] The accuracy of the crystal orientation was approximately 5°.

III. THEORY

Our approach to describe magnetic behavior of the $Ni_5(TeO_3)_4Br_2$ system at different temperatures and in different magnetic fields extends the molecular-field model, which we developed in Ref. 6. The dominant terms of the spin Hamiltonian were determined by taking into account the crystal structure[4] and magnetic structure below $T_N=29$ K.[6] Considering distances between the magnetic Ni^{2+} ($S=1$) moments and the absence of efficient exchange pathways, the interactions between the two subsequent NiTeO layers were neglected and only the exchange between the neighboring ions lying in the same layer was considered. The structure of the individual NiTeO layer suggests six different exchange coupling constants $\underline{J}_{ij}$ between three distinct Ni sites. These reduce to four parameters (see Table I) since for each pair of Ni sites coupled by both the intracluster and the intercluster exchange couplings $\underline{J}_{ij}$, the two couplings constitute a single independent parameter within our molecular-field model.[6] Additional magnetic anisotropy terms are sizable. These include single-ion anisotropies $\underline{D}_j$ for each of the three Ni sites due to severe distortions of the $[NiO_6]$ octahedra and three different Dzyaloshinsky-Moriya antisymmetric exchange interactions $\vec{d}_{ij}$, which are allowed due to the lack of symmetry restrictions.

Low-temperature magnetic structure of the system in the absence of the external magnetic field is known from neutron-diffraction and AFMR studies and can be satisfactorily described with ten sublattice magnetizations in the molecular-field formalism.[6] The spin Hamiltonian is rewritten into magnetic free energy[6] with symmetric exchange interaction between the nearest neighbors, single-ion anisotropy, Dzyaloshinsky-Moriya antisymmetric exchange interaction, and Zeeman term, respectively,

$$F=\sum_{i>j}\vec{M}_i\cdot\underline{A}_{ij}\cdot\vec{M}_j+\sum_j\vec{M}_j\cdot\underline{K}_j\cdot\vec{M}_j+\sum_{i>j}\vec{B}_{ij}\cdot(\vec{M}_i\times\vec{M}_j)$$
$$-\frac{\mu_0}{g_0}\sum_j\vec{M}_j\cdot\underline{g}_j\cdot\vec{H}_0. \quad (1)$$

Here $\vec{M}_j=-N_{\mathrm{sub}}g\mu_B\langle\vec{S}_j\rangle$ stands for jth sublattice magnetization, where N_{sub} is the number of Ni^{2+} magnetic ions on each sublattice, $\underline{g}_j$ is the g-factor tensor, $g_0=2.0023$ is the g factor of the free electron, μ_0 is the vacuum permeability, $\vec{H}_0$ is the applied magnetic field, and $\langle\cdots\rangle$ indicates the thermal average. The molecular-field constants are related to the microscopic parameters through

$$\underline{A}_{ij}=\frac{\underline{J}_{ij}}{N(g\mu_B)^2},$$

$$\underline{K}_j=\frac{\underline{D}_j}{N(g\mu_B)^2},$$

$$\vec{B}_{ij} = \frac{\vec{d}_{ij}}{N(g\mu_B)^2}, \tag{2}$$

where μ_B represents the Bohr magneton. The parameters for the above free energy are summarized in Table I.[6]

The equilibrium orientations of the sublattice magnetizations can be calculated by minimization of the free energy [Eq. (1)] under the assumption that their magnitudes remain constant. To account for the temperature dependence of the magnetic structure we introduce the temperature dependent sublattice magnetizations,[11]

$$M_i(T) = M_i(0)B_S(\mu_B H_{\text{eff}}^{(i)}/k_B T), \tag{3}$$

where $H_{\text{eff}}^{(i)}$ is the effective magnetic field acting on a given sublattice, $B_S(x)$ is the Brillouin function, and $M_i(0)$ is the sublattice magnetization at zero temperature. Based on these values we were able to calculate the expected magnetic structure in different applied magnetic fields and follow the rearrangement of the magnetic moments as a function of the magnetic field and temperature, as explained in Sec. V.

IV. RESULTS

A. Heat-capacity measurements

Heat-capacity measurements were performed in the temperature range between 3 and 120 K in zero field [inset of Fig. 1(a)] and in applied magnetic fields H of 4, 6, and 9 T. In zero field a sharp peak is detected at Néel temperature T_N=29 K, where also the magnetic-susceptibility data indicate long-range AFM ordering.[5,6] We stress that the transition temperature seems to be almost independent of the magnetic field—it only marginally decreases from 28.8(2) K at H=0 T to 28.0(2) K at H=9 T.

Temperature dependence of the heat capacity can be generally described as a sum of three contributions: $C_p = C_{\text{latt}} + C_{\text{short}} + C_{\text{long}}$.[12] Here $C_{\text{latt}} = 9Nk_B(T/\theta_D)^3 \int_0^{T/\theta_D} x^4 e^x/(e^x-1)^2 dx$ stands for a phonon contribution to the heat capacity[13] and is calculated in the Debye approximation with the Debye temperature θ_D as a free parameter, N is the number of atoms in the crystal, and k_B is the Boltzmann constant. Further, $C_{\text{short}} \propto T^{-2}$ corresponds to a high-temperature series expansion of exchange-coupled spin contribution to the entropy[12,14] and describes the increase in the heat capacity due to short-range magnetic correlations far above T_N. Finally, $C_{\text{long}} = B_{\text{SW}} T^{d/n} \int F(\Delta, g, H, T)dx$ is the long-range magnetic-ordering part, contributing below T_N. Here the usual $T^{d/n}$ term for the spin-wave contribution is modified by the integral $\int F(\Delta, g, H, T)dx = \int_{(\Delta + g\mu_B H)/k_B T}^{\infty} \{[x^2 e^x/(e^x-1)^2][x - (\Delta + g\mu_B H)/k_B T]^{1/2}\} dx$,[15] which accounts for the field dependence of the spin-wave gap Δ. Parameter d denotes the magnetic lattice dimensionality, n=1 (n=2) stands for antiferromagnetic (ferromagnetic) systems,[12] and constant B_{SW} depends on the spin-wave stiffness and molar volume of the compound.

In order to determine the temperature dependence of the magnetic heat capacity, i.e., $C_{\text{mag}} = C_{\text{long}} + C_{\text{short}}$, C_{latt} has to be estimated first. Since no diamagnetic isostructural compound is available, we simulated the raw heat-capacity data with C_{latt} well above T_N ($T > 3|\theta|$), where the contribution of C_{short} is expected to be marginal. Unconstrained fit to the above expression for C_{latt} yielded $N = 3.6(1) \times 10^{19}$ and θ_D =240(5) K [see solid line in the inset of Fig. 1(a)], At this point we stress that N is consistent with the number of atoms in the studied crystal and that the Debye temperature is comparable to those found in different Ni alloys.[16,17] We subtracted the lattice contribution from the raw heat-capacity data to obtain the magnetic contribution to the heat capacity C_{mag} [Fig. 1(a)]. The expected peak in C_{mag} at T_N is clearly visible. Further, the magnetic contribution to the heat capacity extends up to $T \sim 70$ K, i.e., well above T_N. This underlines the importance of the magnetic short-range ordering effects and confirms the low dimensionality of $Ni_5(TeO_3)_4Br_2$.

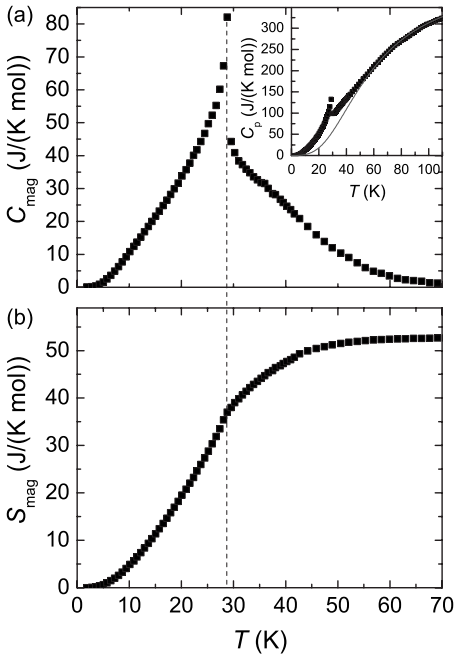

FIG. 1. (a) Temperature dependence of the magnetic heat capacity measured in zero field obtained after subtraction of the phonon contribution from the raw data. Inset: temperature dependence of the heat-capacity raw data (scattered symbols) and the fitted lattice contribution (solid line) with θ_D=240(5) K and $N = 3.6(1) \times 10^{19}$. (b) Integrated magnetic entropy contribution of the zero-field data.

The zero-field data below 7 K can be fitted with the expression for C_{long} (solid line in Fig. 2). In order to reduce the number of free parameters, we assume n=1 (valid for AFM compounds) and d=2 (layered structure). Additionally, we take into account the spin-wave gap obtained from the AFMR measurements, Δ=21.6 K.[6] Hence, B_{SW} remains as the only free parameter and the data simulation leads to B_{SW}=0.0842(1) J/(K^3 mol). The attempt to fit the low-temperature data with d=3 (three-dimensional magnetic structure) failed to satisfactorily describe C_{mag}. We therefore conclude that the intralayer magnetic interactions are dominant in $Ni_5(TeO_3)_4Br_2$ and thus justify our starting assumption of negligible interlayer coupling.[6]

To properly account for the heat-capacity curves in applied magnetic field one should consider increasing population of lower energy states,[18] which is beyond the scope of

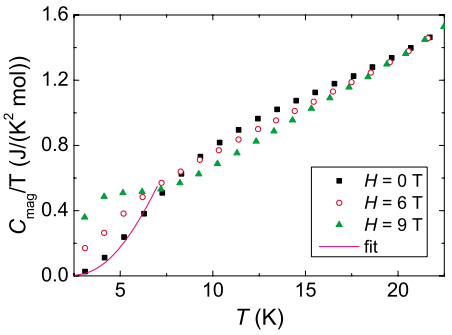

FIG. 2. (Color online) Low-temperature dependences of magnetic contribution to the heat capacity for different magnetic fields: squares for $H=0$ T, circles for $H=6$ T, and triangles for $H=9$ T. Solid line represents the fit for $H=0$ T based on the expression for C_{long}, as described in the text.

the proposed model. We highlight here the appearance of a very broad anomalous bump at $T\approx 10$ K in $H=0$ T data, which shifts to lower T with increasing magnetic field. We tentatively ascribe it to a different temperature evolution of the magnetic moments at different Ni sites, as implied by the temperature evolution of the magnetic peaks in the neutron-diffraction experiment.[6]

The magnetic transition entropy ΔS_{mag} is obtained directly from C_{mag} after calculating the integral,

$$\Delta S_{mag} = \int_0^T C_{mag} d(\ln T). \tag{4}$$

The experimentally obtained total entropy value 52(5) J/(K mol) [Fig. 1(b)] matches with the value $5R\ln(2S+1)=45.7$ J/(K mol) expected for the ordering of full magnetic Ni^{2+} ($S=1$) moments. We stress that a considerable part (~30%) of the magnetic entropy develops at $T > T_N$, implying the importance of short-range ordering effects well above the magnetic transition temperature.

B. Magnetization and magnetic-torque measurements

Adopting two different measuring techniques—direct magnetization and magnetic-torque measurements—we were able to follow the complete response of the magnetization M along the three orthogonal axes $M\|a^*(M_{a^*})$, $M\|b(M_b)$, and $M\|c(M_c)$, with the external magnetic field applied along the a^* crystal axis. The magnetization parallel to the magnetic field, M_{a^*}, was determined from magnetization measurements, which were performed up to 12 T between 1.5 and 10 K (inset of Fig. 3). A well-pronounced inflection point in the $M(H)$ curve can be noticed and is clearly seen as a peak in the derivative dM/dH curves in Fig. 3. The observed maximum of dM/dH is a result of a "spin-flop-like" transition at ~11 T, matching the estimation obtained from the AFMR measurements.[6,8] We notice that the spin-flop-like field shifts with increasing temperature to lower fields and that at the same time the maximum in dM/dH dramatically broadens (Fig. 3). Similar broadening with temperature was observed in the AFMR spectra.[6,9]

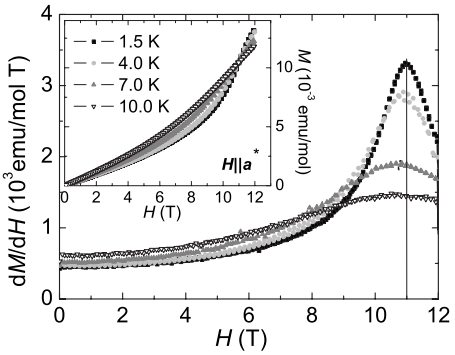

FIG. 3. Derivative of the magnetization curves, dM/dH, measured at different temperatures. Inset: field dependence of the magnetization $M(H)$ (raw data).

To determine the response of the perpendicular magnetization (M_b and M_c) with respect to the applied field, $\vec{H}\|a^*$, magnetic-torque measurements were performed [Figs. 4(a) and 4(b)]. Due to experimental limitations, the magnetic field was applied only perpendicular to the cantilever surface, i.e., parallel to the crystal a^* axis. Hence, the magnetic torque $\tau = \mu_0 \vec{M} \times \vec{H}$ was measured only in b and c directions, which revealed qualitative responses of M_c and M_b, respectively.

The measurements of the magnetic torque parallel to b, indicating the response of the component of the magnetization along the crystal c direction, M_c, show a pronounced change below 29 K, which can be associated with the Néel

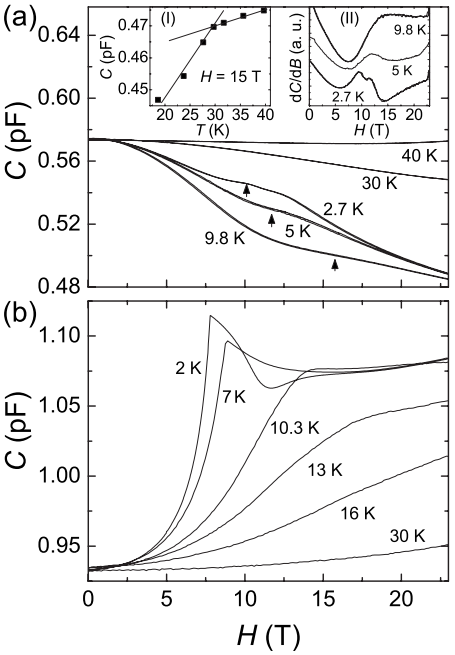

FIG. 4. (a) Field and temperature dependencies of the capacity yielding the magnetic torque in the b direction (indicating the changes in M_c). The arrows reveal the inflection points. Inset (I) shows $C(T)$ at 15 T; straight lines are a guide for the eyes and help indicate the change in $C(T)$ slope. Inset (II) shows the derivative dC/dH curves for typical torque measurements. (b) Field and temperature dependencies of the capacity yielding the magnetic torque in the c direction, indicating the changes in M_b.

transition and is almost field independent up to 23 T. The transition is clearly seen in inset I of Fig. 4(a), where we plot $C(T)$ at 15 T. At lower temperatures (below 10 K), an inflection point is observable in the capacitance curves $C(H)$. This feature is manifested as a peak in the derivative dC/dH curves in inset II of Fig. 4(a). The field corresponding to the peak in these curves is in the range of the spin-flop-like transition[6] and strongly depends on temperature as it shifts from 11.3 T at 3.7 K up to 16 T at 9.8 K. However, below 3.7 K, this peak in dC/dH curve splits and at 2.7 K we observe two well-defined peaks at 9.7 and 11.6 T.

In contrast to the field and temperature dependencies of M_c [Fig. 4(a)], the component of the magnetization along the crystal b axis, M_b, (indicated by the magnetic torque in the c direction) does not exhibit any observable feature when going through the transition from paramagnetic (PM) to AFM states. This observation is consistent with our previous conclusions that in zero field the Ni^{2+} moments order in the a^*-c crystal plane.[6] Below 13 K, we start to observe an exceptionally sharp anomaly superimposed on the otherwise smooth capacity curves [Fig. 4(b)]. The magnetic field, corresponding to this feature, is strongly temperature dependent and monotonically decreases from 14 T at 10.3 K to 7.8 T at 1.8 K.

V. DISCUSSION

The two-dimensional layered structure of $Ni_5(TeO_3)_4Br_2$ would normally emerge as a candidate for geometrically frustrated systems due to the triangular-based geometry of the $[Ni_5O_{17}Br_2]$ basic unit and the competition between the intracluster and intercluster exchange interactions.[4] The previous AFMR, magnetic-susceptibility, and neutron-diffraction measurements[6,8,10] however provided complementary evidences that the presence of a strong magnetic anisotropy suppresses the frustration effects and stabilizes the Néel ground state. Our magnetic heat-capacity data (Fig. 1) indicate the development of short-range magnetic correlations already at temperatures as high as $T\sim 70$ K, i.e., at $\sim 2.3\ T_N$, comparable to the Curie-Weiss temperature $\theta=-50$ K and the strongest exchange interactions $J\sim 56$ K.[6] We believe that the experimental observation of the short-range spin correlations to relatively high temperature with respect to T_N is not related to geometrical frustration but is rather a signature of the two-dimensional nature of the magnetic lattice.

The magnetic heat-capacity measurements, complemented with the magnetization and magnetic-torque measurements in case of the magnetic field applied in the a^* direction, imply, first, a rather complicated noncollinear magnetic structure and, second, an intriguing temperature evolution of individual sublattice magnetizations. In particular, the transition from the PM to the AFM state (hereafter labeled as AFM1 phase) at $T_N=29$ K is seen as a sharp peak in C_{mag} [Fig. 1(a)] and a pronounced change in M_c [inset I of Fig. 4(a)]. This transition is almost independent of the applied magnetic field up to 23 T. Moreover, the heat capacity indicates a very broad bump at $T\approx 10$ K, which rapidly shifts to lower temperatures with increasing field. Further, in agreement with the published AFMR data,[6,8] a spin-flop-like transition is observed as an abrupt change in M_b around 10 T [Fig. 4(b)] as well as in M_{a^*} (Fig. 3) and M_c [Fig. 4(a)], where the corresponding changes are less sharp. The maxima, given by the peaks in the derivatives dM_{a^*}/dH and both dC/dH (indicating the changes in M_b and M_c), seem to occur at slightly different fields.

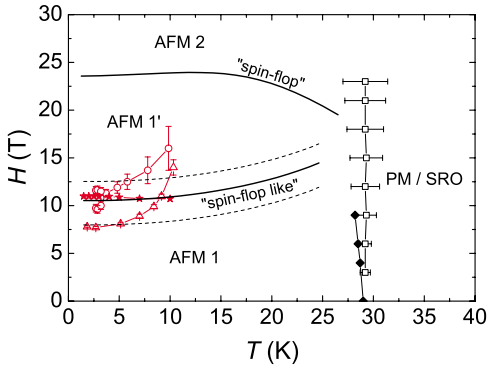

FIG. 5. (Color online) Phase diagram of the $Ni_5(TeO_3)_4Br_2$ compound. Empty circles and triangles stand for the maxima in dC/dH (torque measurements) corresponding to the changes in M_c (circles) and M_b (triangles), solid stars correspond to the peak in dM_{a^*}/dH obtained from magnetization measurements, solid black rhombs represent peaks in the temperature dependence of the heat capacity, and black empty squares represent the sudden change in the $C(T)$ slope obtained from the torque measurements, corresponding to changes in M_c. The solid lines show the transitions predicted by our molecular-field model, while the dashed lines represent the transition-field boundaries obtained when tilting the applied field from the a^* by 5°, which corresponds to the experimental uncertainty of the crystal orientation.

We believe that, at low temperatures, increasing the applied magnetic field along a^* axis above 10 T changes the arrangement of the magnetic moments and causes a transition from the in-plane AFM1 ordering to a more complex high-field AFM1′ ordering, with the magnetic moments canted out of the a^*-c plane. In Fig. 5 we show the corresponding H-T phase diagram of $Ni_5(TeO_3)_4Br_2$ based on our heat-capacity and magnetization measurements. The AFM1-AFM1′ transition is reminiscent of a spin-flop transition for a simple two-sublattice model. It is thus not surprising that it is seen as softening of the lowest AFMR mode. It becomes progressively more hindered with increasing temperature and is not observable any more above 15 K. We note that AFMR signal disappears at the same temperature.[6]

In order to understand how the applied magnetic field affects the spin order at low temperatures, we utilize the molecular-field model presented in Sec. III. Using the parameters [Eq. (2)] given in Table I and minimizing the magnetic free energy [Eq. (1)] for $\vec{H}\|a^*$, the field dependence of the magnetization was calculated. The spin-flop-like transition was determined from the inflection points in the simulated $M(H)$ curves. In the zero-temperature limit the AFM1 to AFM1′ transition is predicted at ~ 10 T (Fig. 5). We stress that the transition field and the broadness of the $dM(H)/dH$ curves were found to be extremely sensitive to the applied magnetic field direction, i.e., deviation of the applied field

for less than 5° causes the transition field to change for more than 1 T. We believe that such enhanced response directly reflects the complexity of the studied system. Thus, we suspect that the shift toward lower fields and the sharpness of the peak in Fig. 4(b) are likely to be of experimental origin. The second peak at 11.6 T in the dC/dH curve at 2.7 K in Fig. 4(a) is beyond the scope of our model and might reflect another transition due to higher order terms in the spin Hamiltonian.

In order to describe the magnetic response of $Ni_5(TeO_3)_4Br_2$ at finite temperatures, we assume the temperature dependence of the sublattice magnetizations M_i, as described in Eq. (3). In the first approximation, we further assume that the exchange interactions and anisotropy constants are temperature independent. As a result, our model correctly predicts that the spin-flop-like field should increase with increasing temperature, matching well with the observed behavior (Fig. 5). We stress that the agreement between the theory and our measurements is particularly decent since all the parameter are fixed based on previous antiferromagnetic resonance and neutron-diffraction studies.

Experimentally, different transition fields were observed for different magnetization components. Taking into account the experimental uncertainty of the crystal orientation (5°), all the measured transition fields up to ~10 K are still within the field region given by our model (dashed lines in Fig. 5, which correspond to the tilt of the applied field from the a^* direction by 5°). Considering that our molecular-field model is valid at low temperatures and that at higher temperatures deviations from the average sublattice magnetization values are increased, discrepancy between the theoretical and experimental results above 10 K, i.e., above $\sim 0.5T_N$, is inevitable. The predicted Néel temperature is 40 K. The model could possibly be improved by introducing temperature-dependent exchange interactions and anisotropy constants—as done similarly in Ref. 11—which would enable a more accurate estimation of the Néel temperature as well as potentially reproduce the observed strong temperature dependence of the spin-flop-like field at higher temperatures.

Lastly, in Fig. 6 we show the calculated zero-temperature magnetic structures for $H=0$, 19, and 30 T. The AFM1 phase, identified by AFMR and neutron-diffraction experiments,[6] consists of antiferromagnetically arranged $[Ni_5O_{17}Br_2]$ clusters [Fig. 6(c)]. In agreement with the magnetization measurements, our simulations suggest that the magnetic structure is almost field independent up to 10 T. Here the Ni^{2+} moments start to bend toward the crystalline b axis, marking the spin-flop-like transition to the AFM1′ phase [Fig. 6(b)]. During this rearrangement, the magnetization component M_b starts to grow. The moments continue their reorientation up to the field of ~24 T, where the magnetic structure again drastically changes. Above this field $Ni_5(TeO_3)_4Br_2$ can be described with another type of magnetic ordering [labeled as AFM2 phase and shown in Fig. 6(a)]. In this phase the arrangement is again almost planar; however, it differs significantly from the AFM1 phase—the intercluster ordering becomes ferromagnetic, with central Ni^{2+} moment inside each cluster still being antiparallel to the other four. Such transition is a clear demonstration of the competition between intracluster and intercluster interactions. For $H>24$ T the external magnetic field suppresses the intercluster AFM interactions but is still weaker than the leading intracluster AFM interactions. The existence of the AFM2 phase, predicted by our simulations for $H>24$ T, requires experimental verification by magnetic measurements in higher fields.

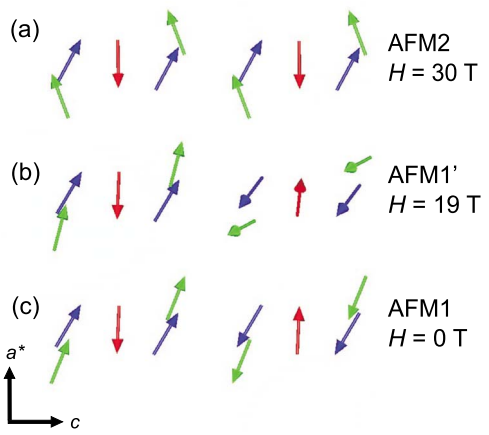

FIG. 6. (Color online) Calculated orientations of all ten sublattice magnetizations in the a-c plane for the magnetic field H applied in the a^* direction (the b axis is pointing out of the paper) for (a) $H=30$ T, (b) $H=19$ T, and (c) $H=0$ T. Red, green, and blue arrows correspond to three nonequivalent sites: Ni1, Ni2, and Ni3, respectively.

VI. CONCLUSION

In summary, our systematic temperature and magnetic field dependent heat-capacity, magnetization, and magnetic-torque measurements allowed us to draw the H-T phase diagram of the two-dimensional $Ni_5(TeO_3)_4Br_2$ compound. The contribution to the magnetic heat capacity observed at temperatures as high as $2.3T_N$ suggests a development of short-range magnetic correlations at rather high temperatures. Additionally, the short-range correlations are enhanced by the quasi-two-dimensional nature of the investigated spin system. Below $T_N=29$ K, the H-T phase diagram is very rich. It consists of a number of low-temperature AFM phases governed by the presence of strong magnetic anisotropies and the competition between the intracluster and intercluster exchange interactions. The zero-field (AFM1) phase is characterized by a planar AFM arrangement of the two in-layer neighboring $[Ni_5O_{17}Br_2]$ magnetic clusters within a magnetic unit cell. When the magnetic field is applied in the a^* crystal direction, the spin-flop-like transition to the AFM1′ phase occurs at approximately 10 T. Here, the magnetic field does not affect all the $[Ni_5O_{17}Br_2]$ clusters in equal manner. The magnetic structure of clusters with the majority of the magnetic moments aligned close to the field direction stays almost intact, whereas the orientations of the Ni^{2+} magnetic moments in the other half of the clusters change from planar to a more complex out-of-plane arrangement. This transition

is shifted to higher fields with increasing temperature, as indicated by our calculations. Finally, a stable AFM phase is predicted above 24 T, where $[Ni_5O_{17}Br_2]$ clusters are ordered ferromagnetically while the intracluster ordering of the central and the four surrounding moments remains antiferromagnetic. To conclude, both our measurements and our modeling show that building of layered systems from strongly coupled clusters might result in an intriguing sequence of AFM structures driven by the applied magnetic field.

ACKNOWLEDGMENTS

M.P. acknowledges helpful discussions with Sophie De Brion concerning the analysis of the torque measurements. This work has been supported by the "Transnational Access to Infrastructure-Specific Support Action" program under Contract No. RITA-CT-2003-505474 of the European Commission.

[1] J. Orenstein and A. J. Millis, Science **288**, 468 (2000), and references therein; E. W. Hudson, K. M. Lang, V. Madhavan, S. H. Pan, H. Eisaki, S. Uchida, and J. C. Davis, Nature (London) **411**, 920 (2001).

[2] R. von Helmolt, J. Wecker, B. Holzapfel, L. Schultz, and K. Samwer, Phys. Rev. Lett. **71**, 2331 (1993); S. Jin, T. H. Tiefel, M. McCormack, R. A. Fastnacht, R. Ramesh, and L. H. Chen, Science **264**, 413 (1994).

[3] P. Lecheminant, B. Bernu, C. Lhuillier, L. Pierre, and P. Sindzingre, Phys. Rev. B **56**, 2521 (1997); C. Waldtmann, H.-E. Everts, B. Bernu, C. Lhuillier, P. Sindzingre, P. Lecheminant, and L. Pierre, Eur. Phys. J. B **2**, 501 (1998).

[4] M. Johnsson, K. W. Tornroos, P. Lemmens, and P. Millet, Chem. Mater. **15**, 68 (2003).

[5] A. Zorko, D. Arčon, J. Dolinšek, Z. Jagličič, A. Jeromen, H. van Tol, L. C. Brunel, and H. Berger, J. Phys.: Condens. Matter **19**, 145278 (2007).

[6] M. Pregelj, A. Zorko, H. Berger, H. van Tol, L. C. Brunel, A. Ozarowski, S. Nellutla, Z. Jagličič, O. Zaharko, P. Tregenna-Piggott, and D. Arčon, Phys. Rev. B **76**, 144408 (2007).

[7] D. Arčon, A. Zorko, M. Pregelj, J. Dolinšek, H. Berger, A. Ozarowski, H. van Tol, and L. C. Brunel, J. Magn. Magn. Mater. **316**, e349 (2007).

[8] L. Mihály, T. Fehér, B. Dóra, B. Náfrádi, H. Berger, and L. Forró, Phys. Rev. B **74**, 174403 (2006).

[9] M. Pregelj, D. Arčon, A. Zorko, L. C. Brunel, H. van Tol, A. Ozarowski, S. Nellutla, and H. Berger, Physica B **403**, 950 (2008).

[10] H. Donavan, *Magnetic Measurements with Metal Film Cantilevers: A Users Guide, Instrumentation & Operations* (HNMFL, Tallahassee, 1999).

[11] S. G. Kaplan, T. W. Noh, A. J. Sievers, S. W. Cheong, and Z. Fisk, Phys. Rev. B **47**, 5300 (1993).

[12] S. Ohkoshi, H. Tokoro, and K. Hashimoto, Coord. Chem. Rev. **249**, 1830 (2005).

[13] N. W. Ashcroft and N. D. Mermin, *Solid State Physics* (Cornell University, Orlando, 1976).

[14] R. L. Carlin, *Magnetochemistry* (Springer-Verlag, Berlin, 1986), p. 41.

[15] R. A. Fisher, F. Bouquet, N. E. Phillips, J. P. Franck, G. Zhang, J. E. Gordon, and C. Marcenat, Phys. Rev. B **64**, 134425 (2001).

[16] R. Tarasenko, A. Orendáčová, K. Tibenská, I. Potočňák, M. Kajňaková, A. Vlček, M. Orendáč, and A. Feher, Acta Phys. Pol. A **113**, 481 (2008).

[17] M. Choi, J. I. Budnick, D. M. Pease, G. H. Hayes, and S. M. Heald, Phys. Rev. B **44**, 9319 (1991).

[18] B. R. Cooper, Proc. Phys. Soc. London **80**, 1225 (1962).